Full halo coronal mass ejections: Do we need to correct the projection effect in terms of velocity?

Chenglong Shen,[1] Yuming Wang,[1] Zonghao Pan,[1] Min Zhang,[1]
Pinzhong Ye,[1] and S. Wang[1]

Received 18 March 2013; revised 13 October 2013; accepted 19 October 2013; published 21 November 2013.

[1] The projection effect is one of the biggest obstacles in learning the real properties of coronal mass ejections (CMEs) and forecasting their geoeffectiveness. To evaluate the projection effect, 86 full halo CMEs (FHCMEs) listed in the Coordinated Data Analysis Workshop CME catalog from 1 March 2007 to 31 May 2012 are investigated. By applying the Graduated Cylindrical Shell model, we obtain the deprojected values of the propagation velocity, direction, and angular width of these FHCMEs and compare them with the projected values measured in the plane-of-sky. Although these CMEs look full halo in the view angle of SOHO, it is found that their propagation directions and angular widths could vary in a large range, implying projection effect is a major reason causing a CME being halo, but not the only one. Furthermore, the comparison of the deprojected and projected velocities reveals that most FHCMEs originating within 45° of the Sun-Earth line with a projected speed slower than 900 km s^{-1} suffer from large projection effect, while the FHCMEs originating far from the vicinity of solar disk center or moving faster than 900 km s^{-1} have small projection effect. Thus, for the latter class of FHCMEs, it is not necessary to correct the measured velocities.

Citation: Shen, C., Y. Wang, Z. Pan, M. Zhang, P. Ye, and S. Wang (2013), Full halo coronal mass ejections: Do we need to correct the projection effect in terms of velocity?, *J. Geophys. Res. Space Physics*, *118*, 6858–6865, doi:10.1002/2013JA018872.

1. Introduction

[2] Halo coronal mass ejections (CMEs), which appear to surround the occulting disk of coronagraphs, were first reported by *Howard et al.* [1982] based on observations from Solwind or P78-1. Since then, the properties and geoeffectiveness of halo CMEs have been widely studied and discussed [e.g., *St. Cyr et al.*, 2000; *Wang et al.*, 2002; *Yashiro et al.*, 2004; *Burkepile et al.*, 2004; *Schwenn et al.*, 2005; *Lara et al.*, 2006; *Gopalswamy*, 2009; *Gopalswamy et al.*, 2007, 2010b; *Temmer et al.*, 2008; *Wang et al.*, 2011; *Cid et al.*, 2012, and reference therein].

[3] Most aforementioned studies were based on the analyses of the observations from single-point observations, such as Solar Maximum Mission, Solar and Heliospheric Observatory (SOHO), etc. However, the projection effect, unavoidable in single-point observations, would significantly distort the real geometric and kinematic parameters of CMEs, especially for full halo CMEs (FHCMEs) which are thought to originate from the vicinity of the solar disk center [e.g., *Howard et al.*, 1985; *Hundhausen*, 1993; *Webb and Howard*, 1994; *Sheeley et al.*, 1999; *Vršnak et al.*, 2007; *Howard et al.*, 2008; *Gao et al.*, 2009; *Temmer et al.*, 2009; *Wang et al.*, 2011]. Various models, such as cone models [e.g., *Zhao et al.*, 2002; *Xie et al.*, 2004; *Xue et al.*, 2005; *Michalek*, 2006; *Zhao*, 2008], and some simple deprojection models [e.g., *Shen et al.*, 2007; *Howard et al.*, 2007, 2008] have been developed to obtain the real parameters of CMEs. Based on a deprojection method, for example, *Howard et al.* [2008] discussed the projection effect on the kinematic properties of CMEs. They found that the corrected values of CME parameters can significantly differ from the projected measurements, and the angular widths of CMEs are correlated with their speeds.

[4] The successful launch of the Solar Terrestrial Relations Observatory (STEREO) [*Kaiser et al.*, 2008] first provided multiple-point observations of CMEs. Based on different assumptions, various models, such as Graduated Cylindrical Shell (GCS) model [*Thernisien et al.*, 2006, 2009; *Thernisien*, 2011], triangulation methods [e.g., *Temmer et al.*, 2009; *Lugaz et al.*, 2009, 2010; *Liu et al.*, 2010; *Lugaz*, 2010; *Liu et al.*, 2012], mask fitting methods [*Feng et al.*, 2012, 2013], Geometric Localisation [*de Koning et al.*, 2009], and Local Correlation Tracking Plus Triangulation [*Mierla et al.*, 2009], were developed. The accuracy and the difference of some models have been compared and discussed by *Lugaz* [2010] and *Feng et al.* [2013]. Since then, the geometric and kinematic parameters of CMEs could be determined in a more reliable way.

[1]CAS Key Laboratory of Geospace Environment, Department of Geophysics and Planetary Sciences, University of Science and Technology of China, Hefei, China.

Corresponding author: C. Shen, CAS Key Laboratory of Geospace Environment, Department of Geophysics and Planetary Sciences, University of Science and Technology of China, Hefei, Anhui 230026, China. (clshen@ustc.edu.cn)

2169-9380/13/10.1002/2013JA018872

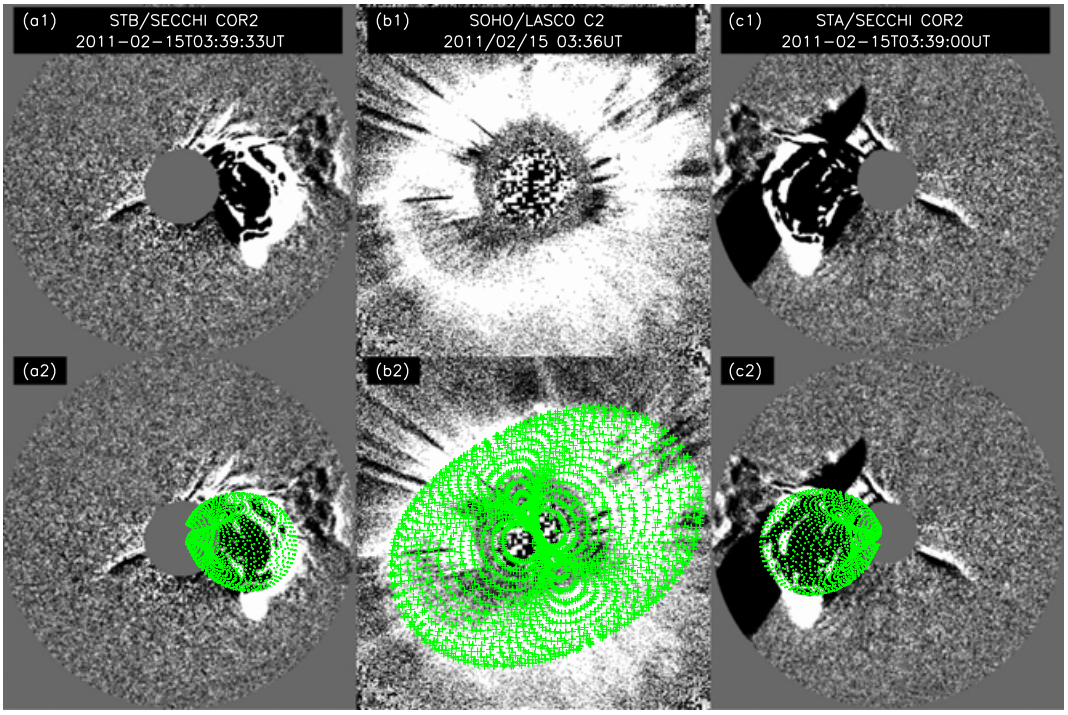

Figure 1. The GCS model's fitting result for 15 February 2011 CME. (a1–c1) the imaging observations of this CME. (a2–c2) the images with the GCS wireframe (green symbols) overlaid on top. From left to right, they are STEREO B, SOHO, and STEREO A observations, respectively.

[5] Since STEREO data will not be available forever, the space weather forecasting will have to rely on single-point observations, from which projected values can be measured. Thus, it is time to reevaluate how significantly the projection effect can influence the CMEs' parameters. Here we are particularly interested in the projection effect in terms of velocity, which is the most important parameter in space weather forecasting. FHCMEs, the most likely Earth-directed ones, are selected for this study. The Coordinated Data Analysis Workshop (CDAW) CME catalog [*Yashiro et al.*, 2004] is used to select events, and the time period is from 1 March 2007 to 31 May 2012, during which STEREO and SOHO observations are all available, and the separation angle between the twin spacecraft of STEREO varied from 1° to 233°. It results in a sample of 86 FHCMEs. In section 2, we will briefly introduce the GCS model and its application to the FHCMEs. The deprojected properties of FHCMEs will be presented in section 3. In section 4, we will show the significance of the projection effect and try to answer the question of which kind of FHCMEs need correction. A summary and conclusions are given in the last section.

2. Method

[6] GCS model is an empirical and forward fitting method to represent the structure of flux rope-like CMEs [*Thernisien et al.*, 2006, 2009; *Thernisien*, 2011] and has proved to be one of the best models to derive real parameters from projected images [e.g., *Liu et al.*, 2010; *Poomvises et al.*, 2010; *Vourlidas et al.*, 2011; *Shen et al.*, 2012, 2013]. The GCS model has six free geometric parameters, which are the propagation longitude ϕ and latitude θ, aspect ratio κ, tilt angle γ with respect to the equator, the half-angle α between the legs, and finally, the height h of the CME leading edge [see *Thernisien et al.*, 2006, Figure 1]. To derive the deprojected parameters of CME, we adjust these six parameters manually to get the best match between the modeled CME and the observed CME in all STEREO and SOHO coronagraphs, i.e., STEREO/COR2 A and B and SOHO/Large Angle and Spectrometric Coronagraph (LASCO). In this procedure, the contrast of images is carefully adjusted to distinguish the main body of CMEs and the associated shock fronts. The STEREO/Sun Earth Connection Coronal and Heliospheric Investigation (SECCHI) COR1 data are not used due to its poor quality.

[7] Figure 1 shows an example of the GCS model's fitting result. We find that there are 80% (69 out of 86) FHCMEs could be well fitted by the GCS model. For a well-fitted CME, a time series of its direction, angular width, and height could be obtained. The CME real speed, $v_{\rm GCS}$, is derived by the linear fitting of the height-time points. To get a more reliable result, we calculate $v_{\rm GCS}$ only for the CMEs recorded in at least three frames. In our sample, there are three CMEs, which appeared in only one or two frames, and therefore the speed cannot be estimated. Table 1 shows the numbers of CMEs in different groups.

[8] Why the 17 CMEs in group III cannot be fitted by the GCS model? We find that there are two reasons: First, the CME pattern is contaminated by other transient structures, which makes the boundary of the CME unclear. Such a phenomenon could be found in 12 events. As an example, Figure 2a shows the 30 July 2007 event. At 06:06 UT, there are probably three CMEs recorded by coronagraphs

Table 1. CME Numbers in Different Groups[a]

Group I	Group II	Group III	Total
66 (59)	3	17	86

[a]Group I: CME is well fitted by GCS model and linear fitting speed v_{GCA} could be obtained. The number in the parentheses is the number of CMEs in which the v_{CDAW} could not be calculated. Group II: CME is well fitted by GCS model, but no speed is available. Group III: CME cannot be fitted by GCS model.

simultaneously. Second, the CME is away from a flux rope-like shape. The other five events are in this case. Figure 2b shows an example which occurred on 31 August 2010. One can see that one part of the CME is much brighter than the other part, especially in the SOHO image. Such a phenomenon is probably due to the presence of ambient streamers or other preexisting CMEs/shocks. Thus, it cannot be the evidence that the CME is not a flux rope-like structure.

[9] An online list is compiled to show the deprojected parameters of these FHCMEs, which could be found at http://space.ustc.edu.cn/dreams/fhcmes/. This list is being continuously updated for new events. It should not be surprising if some most recent events in the online list are not in the sample of this study. In this list, the propagation direction (given by longitude and latitude), the deviation angle (ϵ) between the direction and the Sun-Earth line, the face-on angular width (ω, which is $2(\alpha + \delta)$, in which $\delta = \sin^{-1}\kappa$ is the half-angle of the cone), and the velocity (v_{GCS}) derived from the GCS model are given. The projected speed, v_{CDAW}, is also given for comparison. It should be noted that v_{CDAW} is not simply adapted from the CDAW CME catalog, because the speed it provides is from the measurements of the CME main front in the C2 and C3 field of view (FOV), which is much larger than STEREO COR2's FOV where v_{GCS} is derived. Thus, to make a reasonable comparison between the projected and deprojected speed, we recalculate the projected speed by fitting the height-time measurements provided by the CDAW CME catalog in the FOV of COR2. Note that there are seven events having no v_{CDAW} due to the data points are less than 3.

[10] It should be noted that we only studied the kinematic parameters of the CMEs during their propagation in the field of view of STEREO/COR2. The COR2 instrument observed the corona from 2 to 15 $R_\odot$. Previous results indicated that the acceleration (deceleration) [*Zhang and Dere*, 2006] of CMEs mainly happened in the lower corona region. Thus, we use the constant speed assumption and the discussion about the real acceleration of these CMEs, similar as *Howard et al.* [2008] did, is ignored in this work. In addition, by examining the fitting results for the FHCME events we studied in this paper carefully, we found that almost all the deprojected height-time profiles could be well fitted by straight lines.

3. Deprojected Properties of FHCMEs

[11] Figure 3a shows the distribution of the deviation angle, ϵ, of FHCMEs. It could vary in the full range from about 0° to nearly 90° with an average angle of 35°. Most of them, occupying a fraction of 86% (59 out of 69), are smaller than 50°, and a few of them could be very large. It suggests that the projection effect is indeed the main reason for CMEs being halo, but not always. On the other hand, about 14% (10 out of 69) of FHCMEs are very wide with angular width > 140°. This could be also seen in Figure 3b. Although the

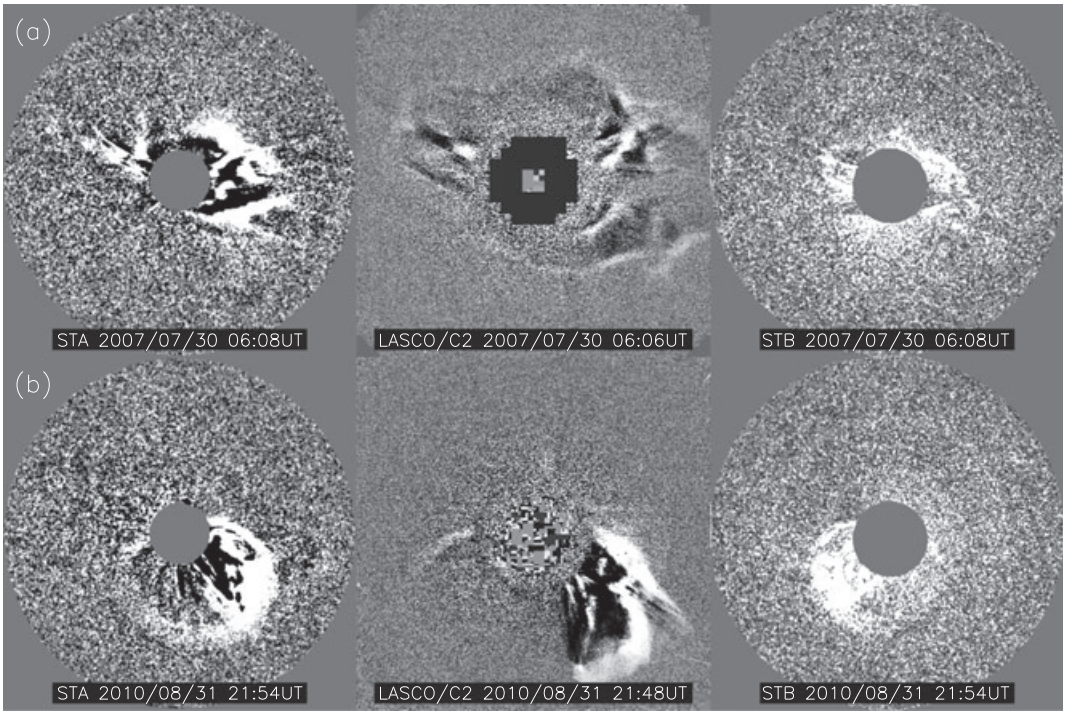

Figure 2. Two examples of the CMEs which could not fitted by the GCS model. (a) the observations for the 30 July 2007 04:54 UT CME and (b) the observations for the 31 August 2010 21:27 UT CME.

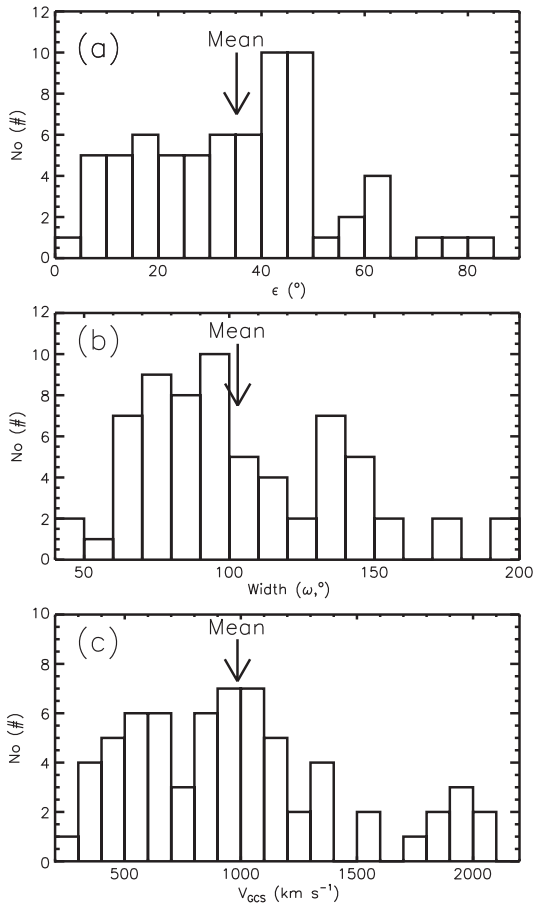

Figure 3. The distribution of the deprojected parameters of the FHCMEs. (a–c) The distribution of the deviation angle (ϵ), angular width (ω), and the deprojected speed ($v_{\rm GCS}$), respectively.

projected angular width of all the CMEs in SOHO/LASCO FOV is all 360°, their real angular width varies in a wide range from as narrow as 44° to as wide as 193°. The average value of the angular width is about 103°, much larger than that of a normal CME, which is about 60° [*Wang et al.*, 2011]. It is found that 45% of FHCMEs are wider than 100°. This fact does imply that FHCMEs consist of a significant number of fast and wide CMEs.

[12] A wider CME tends to be faster. This phenomenon was revealed in previous works by, e.g., *Gopalswamy et al.* [2001], *Yashiro et al.* [2004], *Burkepile et al.* [2004], *Vršnak et al.* [2007], and *Howard et al.* [2008] and also could be seen in Figure 4, which shows the scatterplot between the angular width and $v_{\rm GCS}$. It is found that there is a weak but positive correlation. The correlation coefficient is 0.48 $R_\odot$. A similar correlation can be found in *Vršnak et al.* [2007, Figure 1a] where the projected plane-of-sky velocity and angular width of nonhalo CMEs are compared. Besides, Figure 3c shows the distribution of $v_{\rm GCS}$. The real speeds of these CMEs vary from 274 km s^{-1} to 2016 km s^{-1} with an average speed of 985 km s^{-1}. The difference between the real speeds and projected speeds will be detailedly studied in the next section.

4. Projection Effect of FHCMEs

[13] Projection effect undoubtedly exists for FHCMEs. In terms of space weather forecasting, two parameters, velocity and direction, are the most important. Direction is at secondary place for FHCMEs because most of them may encounter the Earth. The influence of the projection effect of the direction will be briefly discussed in the last section. Here we focus on the first priority parameter, the velocity.

[14] First, we define a parameter to measure the significance of the projection effect in velocity, which is $R_v = \frac{v_{\rm GCS}}{v_{\rm CDAW}}$. In principle, one could expect that R_v should attain a value equal to or larger than unity. $R_v = 1$ means there is no projection effect, while $R_v > 1$ indicates the presence of projection effect. The larger the value of R_v is, the more significant the projection effect is. Figure 5 shows the distribution of R_v, which locates in a range from 0.78 to 2.21.

[15] In this work, the uncertainty of the $v_{\rm GCS}$ comes from the errors of the GCS model's heights and the linear fitting process. *Thernisien et al.* [2009] found that the mean uncertainty in the GCS model's heights is about 0.48 $R_\odot$. By taken this uncertainty into the linear fitting process, we found that the mean relative error of the $v_{\rm GCS}$ is about 12% for these events. It is worth noting that the SOHO/LASCO observations in our study provide an additional constrain on the free parameters. Thus, we believe that the uncertainties of $v_{\rm GCS}$ should be even smaller. For simplicity, a 10% uncertainty is finally applied. The uncertainty of the $V_{\rm CDAW}$ comes from the error in measurements of height of CME's leading edge. Assuming that the error is 0.2 $R_\odot$ (about 4 pixel uncertainty in SOHO/LASCO C3 images), the mean value of the relative error of the $v_{\rm CDAW}$ for these events is 10%. Thus, we use 10% as the uncertainty for both $v_{\rm CDAW}$ and $v_{\rm GCS}$ for all the events in the statistical analysis. We may consider that a value of R_v roughly between 0.8 and 1.2 indicates there is no projection effect. It is found that there are 22 out of 59 events showing obvious projection effect. The velocities of these FHCMEs need to be corrected.

[16] Why do some FHCMEs show significant projection effect and the others not? To answer this question, we investigate the dependence of R_v on the deviation angle ϵ and the projected speed $v_{\rm CDAW}$, which has been shown in

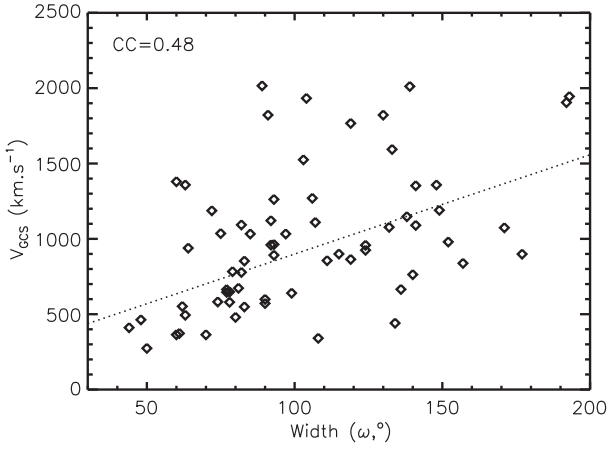

Figure 4. The angular widths of CMEs shown as a function of $v_{\rm GCS}$.

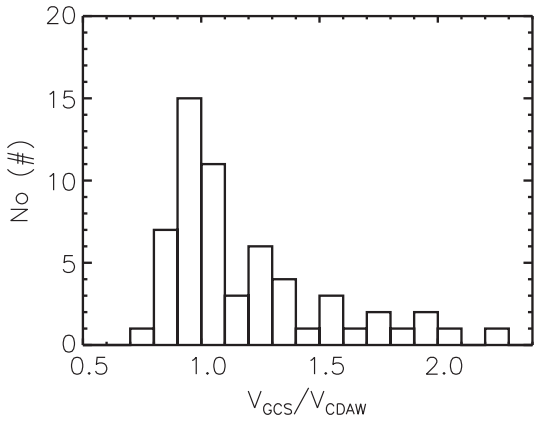

Figure 5. The distribution of the parameter $R_v \left(= \frac{v_{GCS}}{v_{CDAW}}\right)$.

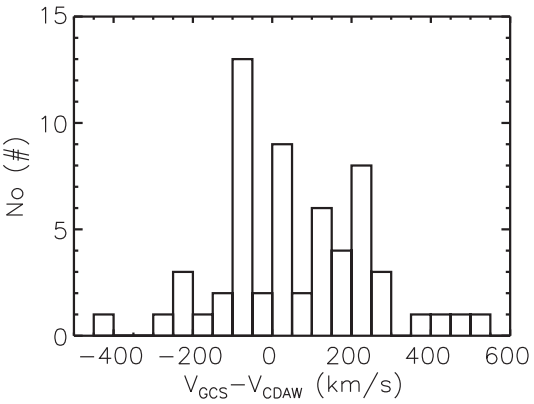

Figure 7. The distribution of the $v_{diff} = v_{GCS} - v_{CDAW}$.

Figure 6. Seen from this figure, a weak correlation between the projected speed and the deviation angle ϵ could be found. A similar correlation was shown in *Vršnak et al.* [2007, Figure 2] in which the location of the CME-related flare (treated as the source region of the CMEs) and the plane-of-sky speeds of these CMEs for nonhalo CMEs were used. In Figure 6, large dots, small dots, and open circles indicate the events with R_v larger than 1.2, between 0.8 and 1.2, and smaller than 0.8, respectively. In addition, the gray scale of the symbols is used to indicate the value of R_v. It can be seen readily that the events with a significant projection effect concentrate in the lower-left corner of the plot. For the events with ϵ larger than 45° or v_{CDAW} larger than 900 km s^{-1}, the values of R_v are all close to unity, except one smaller than 0.8. Thus, we tentatively conclude that all the FFHCMEs which show obvious projection effect ($R_v > 1.2$) are originating within 45° of the Sun-Earth line and moving slower than 900 km s^{-1} in the plane-of-sky. On the other hand, there are total 30 events in the region $\epsilon < 45°$ and $v_{CDAW} < 900$ km s^{-1}, and 73% (22 out of 30) of them have a large value of R_v. These results clearly suggests that, although the projection effect reaches the maximum for FHCMEs, not all of the FHCMEs need to be corrected for the effect in terms of velocity. If assuming CMEs propagate almost radially (though the fact is that CMEs may be deflected during propagation [e.g., *Wang et al.*, 2004, 2006; *Gopalswamy et al.*, 2010a; *Gui et al.*, 2011; *Shen et al.*, 2011; *Zuccarello et al.*, 2012]), the angle ϵ approximately indicates the CME's source location. Then we suggest that the projection effect of FHCMEs originating from the vicinity of solar disk center and not propagating too fast needs to be carefully checked.

[17] The above analysis focuses on the relative difference between v_{GCS} and v_{CDAW}. It should be noted that for a CME with v_{CDAW} larger than 1000 km s^{-1}, 10% uncertainty will lead to an absolute difference larger than 200 km s^{-1} between them. Thus, we further look into the absolute difference between the two velocities, which is $v_{diff} = v_{GCS} - v_{CDAW}$. Figure 7 shows the distribution of v_{diff}. Here we assume a restrict uncertainty of 100 km s^{-1} between the v_{GCS} and v_{CDAW} caused by projection effect. For a CME moving with speed of 1000 km s^{-1}, the 100 km s^{-1} uncertainty leads to an acceptable uncertainty (about 4.6 h) in the CME transit time from the Sun to 1 AU. It is found that there are 26 out of 59 events with $|v_{diff}| < 100$ km s^{-1}, 25 events with v_{GCS} obviously larger than v_{CDAW}, and 8 events with v_{GCS} obviously smaller than v_{CDAW}.

[18] Similarly, the dependence of v_{diff} on ϵ and v_{CDAW} is shown in Figure 8. It could be seen that most (88% or 22 out

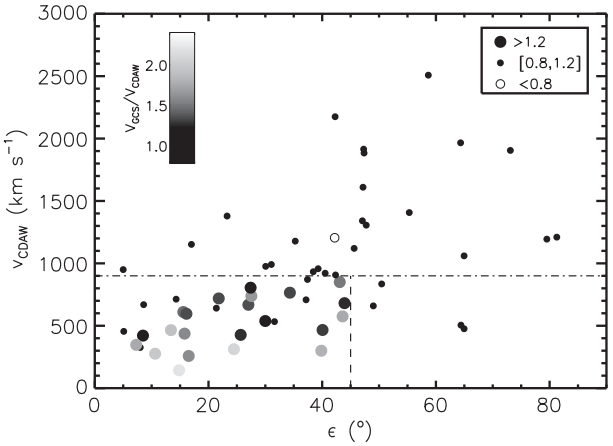

Figure 6. Projected speed shown as a function of the angle ϵ. The gray scale of the symbol indicate the difference value of the R_v.

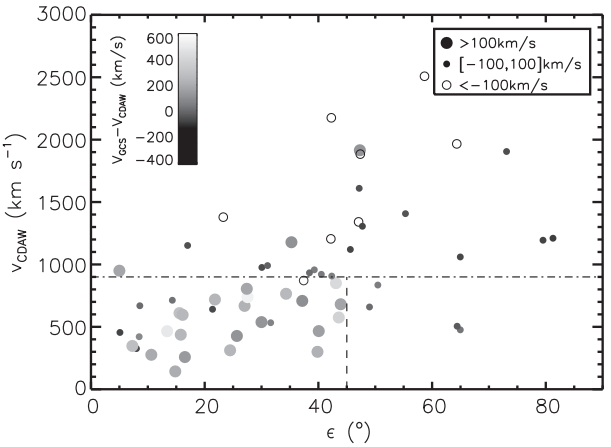

Figure 8. The projected speed varied with the angle ϵ. The gray scale of the symbol indicates the difference value of v_{diff}.

of 25) events with $v_{diff} > 100$ km s^{-1} locate in the lower left corner. If the same thresholds were selected as we have done in Figure 6, i.e., $\epsilon \leq 45°$ and $v_{CDAW} \leq 900$ km s^{-1}, we find that 73% (22 out of 30) of the events in the region have significant projection effect, and on the other hand, 90% (26 out of 29) of the events outside the region do not show obvious projection effect. These results are quite similar to those by using R_v, and further confirm that the velocities of the FHCMEs originating from the vicinity of solar disk center and not propagating too fast are probably influenced by the projection effect.

[19] For the events with $v_{GCS} < v_{CDAW}$, there are several reasons. First, the errors in the measurements and fitting procedures are large. Second, v_{GCS} is derived by fitting CME's outline, while v_{CDAW} comes from the measurements of CME's leading edge along a certain direction. The latter may probably be a shock rather than the CME body. We notice that all the CMEs with $v_{diff} < -100$ km s^{-1} are faster than 850 km s^{-1} (particularly, 7 out of 8 CMEs are faster than 1200 km s^{-1}). Such fast CMEs probably drive a shock and can be only recorded in a few frames by coronagraphs. Third, the overexpansion [e.g., *MacQueen and Cole*, 1985; *Moore et al.*, 2007; *Patsourakos et al.*, 2010] and the effect of aerodynamic drag [e.g., *Chen*, 1996; *Cargill*, 2004; *Vršnak and Žic*, 2007; *Vršnak et al.*, 2008; *Lugaz and Kintner*, 2012; *Vršnak et al.*, 2012] might also play a significant role. *Schwenn et al.* [2005] found that the lateral expansion speed may larger than the radial speed with a factor of 1.2. In the projected image, it is hard to distinguish the expansion speed and the propagation speed of a CME. It is possible that the velocity determined in the projected observations might be combined with the real expansion speed and the projected propagation speed. Thus, in cases where the expansion speeds are larger than their radial propagation speeds, their projected speeds might be larger than their real propagation speeds. In addition, different values of the background solar-wind speed at different latitudes might also cause the velocities of some parts of a CME to be faster than the propagation velocity of its front due to the solar-wind drag. Thus, the apparent velocity which measured the fastest part of a CME on the plane-of-sky might be faster than the real propagation velocity.

5. Summary and Conclusion

[20] With the aids of GCS model, we investigate the deprojected parameters of the 69 FHCMEs from 1 March 2007 to 31 May 2012 based on the STEREO/COR2 and SOHO/LASCO observations. It is found that

[21] 1. A large fraction ($\sim$ 80%) of the FHCMEs could be fitted by the CGS model which assumes a flux rope geometry of a CME. Those FHCMEs that cannot be well fitted are probably due to the contamination/distortion by other structures. This result suggests that most CMEs are a flux rope-like structure. It consists with recent studies which argued that all (or large fraction of) CMEs are flux rope structures based on remote or in situ observations [e.g., *Vourlidas et al.*, 2013; *Xie et al.*, 2013; *Yashiro et al.*, 2013; *Zhang et al.*, 2013, and reference therein]. Thus, models which treat the CME as a flux rope [e.g., *Chen*, 1996; *Hu et al.*, 2013; *Hu and Dasgupta*, 2006; *Wang et al.*, 2009] are appropriate to study CMEs.

[22] 2. Although the CMEs we chosen are all full halo CMEs in the view angle of SOHO, the deprojected angular width varies in a large range from 44° to 193°. Moreover, about 30% of front-side FHCMEs have $\epsilon > 45°$, suggesting they are not Earth-directed. For those CMEs with large ϵ and small angular width, it is hard to expect that they would arrive at the Earth. Thus, if we simply use the front side and full halo as criterion to determine Earth-directed CMEs, some wrong alerts will be made. In addition, the ratio of the Earth-direct CMEs arrival to the Earth might be underestimated if we simply use this criterion to determine the Earth-direct CME. However, some questions are still remained for these CMEs: (1) Whether all these Earth-direct FHCMEs arrived at the Earth? (2) Can the "limb" front-side FHCMEs arrive at the Earth? (3) Is there any criterion that could be used to forecast whether a CME will arrive at the Earth or not? Such questions have been widely discussed in the frame of projection parameters [e.g., *Gopalswamy et al.*, 2007; *Zhang et al.*, 2007], and our study represents a step forward in answering these questions.

[23] 3. Not all the FHCMEs show obvious projection effect on the speed. Our results show that the FHCMEs originating within $\epsilon = 45°$ of the Sun-Earth line and moving with a projected speed slower than 900 km s^{-1} probably have obvious projection effect on the speed. Although the twin STEREO spacecraft allow us to obtain the deprojected parameters, they will not always be there and it is quite possible that CMEs can be only observed from one point. Thus, the criterion obtained above is particularly useful for us to determine whether or not a CME needs to correct projection effect, as the two parameters ϵ and v_{CDAW} applied in this criterion could be easily estimated from a single-point observations. Why is the projection effect small for not on-disk ($\epsilon > 45°$) or fast ($v_{CDAW} > 900$ km s^{-1}) CMEs? A possible reason is that, these CMEs are usually wide enough to intersect with the plane of the sky. In this case, the measured velocity of the FHCMEs based on the projected coronagraph images may be close to their real propagation velocity because the fronts of CMEs are nearly circular.

[24] **Acknowledgments.** We acknowledge the use of CME catalog, the data from SECCHI instruments on STEREO and LASCO on SOHO. The CME catalog is generated and maintained at the CDAW Data Center by NASA and the Catholic University of America in cooperation with the Naval Research Laboratory. STEREO is the third mission in NASA Solar Terrestrial Probes program, and SOHO is a mission of international cooperation between ESA and NASA. We also acknowledge the NSSDC at Goddard Space Flight Center/NASA for providing Wind and ACE data. We benefited from discussions with X.P. Zhao. This work is supported by the Chinese Academy of Sciences (KZZD-EW-01), grants from the 973 key project 2011CB811403, NSFC 41131065, 41274173, 40874075, and 41121003, CAS the 100 talent program, KZCX2-YW-QN511 and startup fund, and MOEC 20113402110001, and the fundamental research funds for the central universities (WK2080000031).

[25] Philippa Browning thanks the reviewers for their assistance in evaluating this paper.

References

Burkepile, J. T., A. J. Hundhausen, A. L. Stanger, O. C. St. Cyr, and J. A. Seiden (2004), Role of projection effects on solar coronal mass ejection properties: 1. A study of CMEs associated with limb activity, *J. Geophys. Res.*, *109*, A03103, doi:10.1029/2003JA010149.

Cargill, P. J. (2004), On the aerodynamic drag force acting on interplanetary coronal mass ejections, *Sol. Phys.*, *221*, 135–149.

Chen, J. (1996), Theory of prominence eruption and propagation: Interplanetary consequences, *J. Geophys. Res.*, *101*(A12), 27,499–27,520.

Cid, C., et al. (2012), Can a halo CME from the limb be geoeffective?, *J. Geophys. Res.*, *117*, A11102, doi:10.1029/2012JA017536.

de Koning, C. A., V. J. Pizzo, and D. A. Biesecker (2009), Geometric localization of CMEs in 3D space using STEREO beacon data: First results, *Sol. Phys.*, *256*(1-2), 167–181.

Feng, L., B. Inhester, Y. Wei, W. Q. Gan, T.-L. Zhang, and M. Y. Wang (2012), Morphological evolution of a three-dimensional coronal mass ejection cloud reconstructed from three viewpoints, *Astrophys. J.*, *751*(1), 18, doi:10.1088/0004-637X/751/1/18.

Feng, L., B. Inhester, and M. Mierla (2013), Comparisons of CME morphological characteristics derived from five 3D reconstruction methods, *Sol. Phys.*, *282*(1), 221–238.

Gao, P.-X., K.-J. Li, and Q.-X. Li (2009), Kinetic properties of coronal mass ejections corrected for the projection effect in Cycle 23, *Mon. Not. R. Astron. Soc.*, *394*(2), 1031–1036.

Gopalswamy, N. (2009), Halo coronal mass ejections and geomagnetic storms, *Earth Planets Space*, *61*, 1–3.

Gopalswamy, N., S. Yashiro, M. L. Kaiser, R. A. Howard, and J.-L. Bougeret (2001), Characteristics of coronal mass ejections associated with long-wavelength type II radio bursts, *J. Geophys. Res.*, *106*, 29,219–29,229.

Gopalswamy, N., S. Yashiro, and S. Akiyama (2007), Geoeffectiveness of halo coronal mass ejections, *J. Geophys. Res.*, *112*, A06112, doi:10.1029/2006JA012149.

Gopalswamy, N., P. Mäkelä, H. Xie, S. Akiyama, and S. Yashiro (2010a), Solar sources of "driverless" interplanetary shocks, in *Twelfth International Solar Wind Conference, AIP Conf. Proc., 1216*, 452.

Gopalswamy, N., S. Yashiro, H. Xie, S. Akiyama, and P. Mäkelä (2010b), Large geomagnetic storms associated with limb halo coronal mass ejections, *Adv. Geosci.*, *21*, 71–83.

Gui, B., C. Shen, Y. Wang, P. Ye, J. Liu, S. Wang, and X. Zhao (2011), Quantitative analysis of CME deflections in the corona, *Sol. Phys.*, *271*, 111–139.

Howard, R. A., D. J. Michels, N. R. Sheeley Jr., and M. J. Koomen (1982), The observation of a coronal transient directed at Earth, *Astrophys. J.*, *263*(2), L101–L104.

Howard, R. A., N. R. Sheeley Jr., M. J. Koomen, and D. J. Michels (1985), Coronal mass ejections: 1979–1981, *J. Geophys. Res.*, *90*, 8173–8191.

Howard, T. A., C. D. Fry, J. C. Johnston, and D. F. Webb (2007), On the evolution of coronal mass ejections in the interplanetary medium, *Astrophys. J.*, *667*, 610–625.

Howard, T. A., D. Nandy, and A. C. Koepke (2008), Kinematic properties of solar coronal mass ejections: Correction for projection effects in spacecraft coronagraph measurements, *J. Geophys. Res.*, *113*, A01104, doi:10.1029/2007JA012500.

Hu, Q., and B. Dasgupta (2006), A new approach to modeling non-force free coronal magnetic field, *Geophys. Res. Lett.*, *33*, L15106, doi:10.1029/2006GL026952.

Hu, Q., C. J. Farrugia, V. A. Osherovich, C. Möstl, A. Szabo, K. W. Ogilvie, and R. P. Lepping (2013), Effect of electron pressure on the Grad-Shafranov reconstruction of interplanetary coronal mass ejections, *Sol. Phys.*, *284*, 275–291.

Hundhausen, A. J. (1993), Sizes and locations of coronal mass ejections: SMM observations from 1980 and 1984–1989, *J. Geophys. Res.*, *98*(A8), 13,177–13,200.

Kaiser, M. L., T. A. Kucera, J. M. Davila, O. C. St. Cyr, M. Guhathakurta, and E. Christian (2008), The STEREO mission: An introduction, *Space Sci. Rev.*, *136*(1-4), 5–16.

Lara, A., N. Gopalswamy, H. Xie, E. Mendoza-Torres, R. Pérez-Eríquez, and G. Michalek (2006), Are halo coronal mass ejections special events?, *J. Geophys. Res.*, *111*, A06107, doi:10.1029/2005JA011431.

Liu, Y., A. Thernisien, J. G. Luhmann, A. Vourlidas, J. A. Davies, R. P. Lin, and S. D. Bale (2010), Reconstructing coronal mass ejections with coordinated imaging and in situ observations: Global Structure, kinematics, and implications for space weather forecasting, *Astrophys. J.*, *722*(2), 1762–1777.

Liu, Y. D., et al. (2012), Interactions between coronal mass ejections viewed in coordinated imaging and in situ observations, *Astrophys. J. Lett.*, *746*(2), L15, doi:10.1088/2041-8205/746/2/L15.

Lugaz, N. (2010), Accuracy and limitations of fitting and stereoscopic methods to determine the direction of coronal mass ejections from heliospheric imagers observations, *Sol. Phys.*, *267*(2), 411–429.

Lugaz, N., and P. Kintner (2012), Effect of solar wind drag on the determination of the properties of coronal mass ejections from heliospheric images, *Sol. Phys.*, *285*, 281–294.

Lugaz, N., A. Vourlidas, and I. I. Roussev (2009), Deriving the radial distances of wide coronal mass ejections from elongation measurements in the heliosphere - Application to CME-CME interaction, *Ann. Geophys.*, *27*(9), 3479–3488.

Lugaz, N., J. N. Hernandez-Charpak, I. I. Roussev, C. J. Davis, A. Vourlidas, and J. A. Davies (2010), Determining the azimuthal properties of coronal mass ejections from multi-spacecraft remote-sensing observations with STEREO SECCHI, *Astrophys. J.*, *715*(1), 493–499.

MacQueen, R. M., and D. M. Cole (1985), Broadening of looplike solar coronal transients, *Astrophys. J.*, *299*(1), 526–535.

Michalek, G. (2006), An asymmetric cone model for halo coronal mass ejections, *Sol. Phys.*, *237*(1), 101–118.

Mierla, M., B. Inhester, C. Marqué, L. Rodriguez, S. Gissot, A. N. Zhukov, D. Berghmans, and J. Davila (2009), On 3D reconstruction of coronal mass ejections: I. Method description and application to SECCHI-COR data, *Sol. Phys.*, *259*(1-2), 123–141.

Moore, R. L., A. C. Sterling, and S. T. Suess (2007), The width of a solar coronal mass ejection and the source of the driving magnetic explosion: A test of the standard scenario for CME production, *Astrophys. J.*, *668*(2), 1221–1231.

Patsourakos, S., A. Vourlidas, and G. Stenborg (2010), The genesis of an impulsive coronal mass ejection observed at ultra-high cadence by AIA on SDO, *Astrophys. J. Lett.*, *724*(2), L188–L193.

Poomvises, W., J. Zhang, and O. Olmedo (2010), Coronal mass ejection propagation and expansion in three-dimensional space in the heliosphere based on STEREO/SECCHI observations, *Astrophys. J. Lett.*, *717*, L159–L163.

Schwenn, R., A. Dal Lago, E. Huttunen, and W. D. Gonzalez (2005), The association of coronal mass ejections with their effects near the Earth, *Ann. Geophys.*, *23*(3), 1033–1059.

Sheeley, N. R. Jr., J. H. Walters, Y.-M. Wang, and R. A. Howard (1999), Continuous tracking of coronal outflows: Two kinds of coronal mass ejections, *J. Geophys. Res.*, *104*(A11), 24,739–24,768.

Shen, C., Y. Wang, P. Ye, X. P. Zhao, B. Gui, and S. Wang (2007), Strength of coronal mass ejection-driven shocks near the sun and their importance in predicting solar energetic particle events, *Astrophys. J.*, *670*(1), 849–856.

Shen, C., Y. Wang, B. Gui, P. Ye, and S. Wang (2011), Kinematic evolution of a slow CME in corona viewed by STEREO-B on 8 October 2007, *Sol. Phys.*, *269*(2), 389–400.

Shen, C., G. Li, X. Kong, J. Hu, X. D. Sun, L. Ding, Y. Chen, Y. Wang, and L. Xia (2013), Compound twin coronal mass ejections in the 2012 May 17 GLE event, *Astrophys. J.*, *763*(2), 114, doi:10.1088/0004-637X/763/2/114.

Shen, C., Y. Wang, S. Wang, Y. Liu, R. Liu, A. Vourlidas, B. Miao, P. Ye, J. Liu, and Z. Zhou (2012), Super-elastic collision of large-scale magnetized plasmoids in the heliosphere, *Nat. Phys.*, *8*(1), 923–928.

St. Cyr, O. C., et al. (2000), Properties of coronal mass ejections: SOHO LASCO observations from January 1996 to June 1998, *J. Geophys. Res.*, *105*(A8), 18,169–18,185.

Temmer, M., A. M. Veronig, B. Vršnak, J. Rybák, P. Gömöry, S. Stoiser, and D. Maričić (2008), Acceleration in fast halo CMEs and synchronized flare HXR bursts, *Astrophys. J.*, *673*(1), L95–L98.

Temmer, M., S. Preiss, and A. M. Veronig (2009), CME projection effects studied with STEREO/COR and SOHO/LASCO, *Sol. Phys.*, *256*(1-2), 183–199.

Thernisien, A. (2011), Implementation of the graduated cylindrical shell model for the three-dimensional reconstruction of coronal mass ejections, *Astrophys. J. Suppl. Ser.*, *194*(2), 33, doi:10.1088/0067-0049/194/2/33.

Thernisien, A., A. Vourlidas, and R. A. Howard (2009), Forward modeling of coronal mass ejections using STEREO/SECCHI data, *Sol. Phys.*, *256*(1-2), 111–130.

Thernisien, A. F. R., R. A. Howard, and A. Vourlidas (2006), Modeling of flux rope coronal mass ejections, *Astrophys. J.*, *652*, 763–773.

Vourlidas, A., R. Colaninno, T. Nieves-Chinchilla, and G. Stenborg (2011), The first observation of a rapidly rotating coronal mass ejection in the middle corona, *Astrophys. J.*, *733*(2), L23, doi:10.1088/2041-8205/733/2/L23.

Vourlidas, A., B. J. Lynch, R. A. Howard, and Y. Li (2013), How many CMEs have flux ropes? Deciphering the signatures of shocks, flux ropes, and prominences in coronagraph observations of CMEs, *Sol. Phys.*, *284*(1), 179–201.

Vršnak, B., and T. Žic (2007), Transit times of interplanetary coronal mass ejections and the solar wind speed, *Astron. Astrophys.*, *472*(3), 937–943.

Vršnak, B., D. Sudar, D. Ruždjak, and T. Žic (2007), Projection effects in coronal mass ejections, *Astron. Astrophys.*, *469*(1), 339–346.

Vršnak, B., D. Vrbanec, and J. Čalogović (2008), Dynamics of coronal mass ejections. The mass-scaling of the aerodynamic drag, *Astron. Astrophys.*, *490*(2), 811–815.

Vršnak, B., et al. (2012), Propagation of interplanetary coronal mass ejections: The drag-based model, *Sol. Phys.*, *285*(1-2), 295–315.

Wang, Y. M., P. Z. Yee, S. Wang, G. P. Zhou, and J. Wang (2002), A statistical study on the geoeffectiveness of Earth-directed coronal mass ejections from March 1997 to December 2000, *J. Geophys. Res.*, *107*(A11), 1340, doi:10.1029/2002JA009244.

Wang, Y., C. Shen, S. Wang, and P. Ye (2004), Deflection of coronal mass ejection in the interplanetary medium, *Sol. Phys.*, *222*, 329–343.

Wang, Y., X. Xue, C. Shen, P. Ye, S. Wang, and J. Zhang (2006), Impact of major coronal mass ejections on geospace during 2005 September 7–13, *Astrophys. J.*, *646*, 625–633.

Wang, Y., J. Zhang, and C. Shen (2009), An analytical model probing the internal state of coronal mass ejections based on observations of their expansions and propagations, *J. Geophys. Res.*, *114*, A10104, doi:10.1029/2009JA014360.

Wang, Y., C. Chen, B. Gui, C. Shen, P. Ye, and S. Wang (2011), Statistical study of coronal mass ejection source locations: Understanding CMEs viewed in coronagraphs, *J. Geophys. Res.*, *116*, A04104, doi:10.1029/2010JA016101.

Webb, D. F., and R. A. Howard (1994), The solar cycle variation of coronal mass ejections and the solar wind mass flux, *J. Geophys. Res.*, *99*, 4201–4220.

Xie, H., L. Ofman, and G. Lawrence (2004), Cone model for halo CMEs: Application to space weather forecasting, *J. Geophys. Res.*, *109*, A03109, doi:10.1029/2003JA010226.

Xie, H., N. Gopalswamy, and O. C. St. Cyr (2013), Near-sun flux-rope structure of CMEs, *Sol. Phys.*, *284*(1), 47–58.

Xue, X. H., C. B. Wang, and X. K. Dou (2005), An ice-cream cone model for coronal mass ejections, *J. Geophys. Res.*, *110*, A08103, doi:10.1029/2004JA010698.

Yashiro, S., N. Gopalswamy, G. Michalek, O. C. St. Cyr, S. P. Plunkett, N. B. Rich, and R. A. Howard (2004), A catalog of white light coronal mass ejections observed by the SOHO spacecraft, *J. Geophys. Res.*, *109*, A07105, doi:10.1029/2003JA010282.

Yashiro, S., N. Gopalswamy, P. Mäkelä, and S. Akiyama (2013), Post-eruption arcades and interplanetary coronal mass ejections, *Sol. Phys.*, *284*(1), 5–15.

Zhang, J., and K. P. Dere (2006), A statistical study of main and residual accelerations of coronal mass ejections, *Astrophys. J.*, *649*, 1100–1109.

Zhang, J., et al. (2007), Solar and interplanetary sources of major geomagnetic storms ($Dst \leq -100$ nT) during 1996–2005, *J. Geophys. Res.*, *112*, A10102, doi:10.1029/2007JA012321.

Zhang, J., P. Hess, and W. Poomvises (2013), A comparative study of coronal mass ejections with and without magnetic cloud structure near the Earth: Are all interplanetary CMEs flux ropes?, *Sol. Phys.*, *284*(1), 89–104.

Zhao, X. P. (2008), Inversion solutions of the elliptic cone model for disk frontside full halo coronal mass ejections, *J. Geophys. Res.*, *113*, A02101, doi:10.1029/2007JA012582.

Zhao, X. P., S. P. Plunkett, and W. Liu (2002), Determination of geometrical and kinematical properties of halo coronal mass ejections using the cone model, *J. Geophys. Res.*, *107*(A8), 1223, doi:10.1029/2001JA009143.

Zuccarello, F. P., A. Bemporad, C. Jacobs, M. Mierla, S. Poedts, and F. Zuccarello (2012), The role of streamers in the deflection of coronal mass ejections: Comparison between STEREO three-dimensional reconstructions and numerical simulations, *Astrophys. J.*, *744*(1), 66, doi:10.1088/0004-637X/744/1/66.